Monthly Notices of the ROYAL ASTRONOMICAL SOCIETY
MNRAS **465,** 1274–1288 (2017) doi:10.1093/mnras/stw2730

Photometric properties of intermediate-redshift Type Ia supernovae observed by the Sloan Digital Sky Survey-II Supernova Survey

N. Takanashi,[1⋆] M. Doi,[2,3,4⋆] N. Yasuda,[3⋆] H. Kuncarayakti,[5,6] K. Konishi,[7] D. P. Schneider,[8,9] D. Cinabro[10] and J. Marriner[11]

[1]*Executive Management Program, University of Tokyo, 7-3-1 Hongo, Bunkyo-ku, Tokyo 113-8654, Japan*
[2]*Institute of Astronomy, Graduate School of Science, University of Tokyo, 2-21-1 Osawa, Mitaka, Tokyo 181-0015, Japan*
[3]*Kavli Institute for the Physics and Mathematics of the Universe, University of Tokyo, 5-1-5 Kashiwanoha, Kashiwa, Chiba 277-8568, Japan*
[4]*Research Center for the Early Universe, Graduate School of Science, University of Tokyo, Bunkyo-ku, Tokyo 113-0033, Japan*
[5]*Millennium Institute of Astrophysics, Santiago, Chile*
[6]*Departamento de Astronomía, Universidad de Chile, Casilla 36-D, Santiago, Chile*
[7]*Nikon Corporation, 471, Nagaodai-cho, Sakae-ku, Yokohama, Kanagawa 244-8533, Japan*
[8]*Department of Astronomy and Astrophysics, Pennsylvania State University, University Park, PA 16802, USA*
[9]*Institute for Gravitation and the Cosmos, Pennsylvania State University, University Park, PA 16802, USA*
[10]*Department of Physics and Astronomy, Wayne State University, Detroit, MI 48202, USA*
[11]*Center for Particle Astrophysics, Fermi National Accelerator Laboratory, Batavia, IL 60510, USA*

Accepted 2016 October 20. Received 2016 October 19; in original form 2016 February 15

ABSTRACT

We have analysed multiband light curves of 328 intermediate-redshift ($0.05 \leq z < 0.24$) Type Ia supernovae (SNe Ia) observed by the Sloan Digital Sky Survey-II Supernova Survey. The multiband light curves were parametrized by using the multiband stretch method, which can simply parametrize light-curve shapes and peak brightness without dust extinction models. We found that most of the SNe Ia that appeared in red host galaxies ($u - r > 2.5$) do not have a broad light-curve width and the SNe Ia that appeared in blue host galaxies ($u - r < 2.0$) have a variety of light-curve widths. The Kolmogorov–Smirnov test shows that the colour distribution of SNe Ia appearing in red/blue host galaxies is different (a significance level of 99.9 per cent). We also investigate the extinction law of host galaxy dust. As a result, we find that the value of R_v derived from SNe Ia with medium light-curve widths is consistent with the standard Galactic value, whereas the value of R_v derived from SNe Ia that appear in red host galaxies becomes significantly smaller. These results indicate that there may be two types of SNe Ia with different intrinsic colours, and that they are obscured by host galaxy dust with two different properties.

Key words: supernovae: general – dust, extinction – galaxies: ISM.

1 INTRODUCTION

Type Ia supernovae (SNe Ia) are known as excellent standard candles for tracing the expansion history of the Universe because of their homogeneity and high luminosity (Filippenko 2005). Since the early 1990s, several SNe Ia search programmes have been carried out, which have aimed to measure the Hubble constant. The CALAN/TOLOLO Supernova Search, which started in 1990 (Hamuy et al. 1993, 1995; Phillips 1993), succeeded in producing a moderately distant ($0.01 < z < 0.10$) sample of SNe Ia. The Supernova Cosmology Project (SCP) and the High-Z Team (HZT) are independent high-redshift ($z \sim 0.5$) SN searches designed to measure the cosmological parameters of the Universe. After a careful analysis of their observed SNe Ia, both SCP and HZT reported the accelerating expansion of the Universe (Riess et al. 1998; Schmidt et al. 1998; Perlmutter et al. 1999). This result implies that there is an unknown component in the Universe, called dark energy.

As described above, SNe Ia show properties that are more homogeneous than those of any other astronomical objects, which can be used as standard candles at cosmological distances. However, many studies have also revealed an intrinsic diversity of SN Ia properties. For example, there are several subgroups of SNe Ia that are classified by spectral features. SN1991T-type and SN1991bg-type are well-studied subgroups of SNe Ia (Branch, Fisher & Nugent 1993; Nugent et al. 1995). The SN1991T-type SN Ia has a slightly broader light-curve width and brighter peak magnitude than a normal SN Ia (Phillips et al. 1992). The SN1991bg-type SN Ia has a narrower light-curve width and fainter peak magnitude than a normal SN Ia (Filippenko et al. 1992; Leibundgut et al. 1993).

⋆E-mail: naohiro.takanashi@emp.u-tokyo.ac.jp (NT); doi@ioa.s.u-tokyo.ac.jp (MD); yasuda@icrr.u-tokyo.ac.jp (NY)

We can also find intrinsic diversity in the spectra of SNe Ia without including any obviously SN1991T-like and SN1991bg-like SNe (e.g. Benetti et al. 2005). Recent studies have reported that even spectroscopically normal SNe Ia (called the branch normal; Branch et al. 1993) may have subgroups. In order to describe the observed SN Ia rate, Mannucci et al. (2005) proposed that the population of SNe Ia consists of two components: one called 'prompt', whose rate is proportional to the star formation rate and is possibly related to a young progenitor; the other called 'tardy', whose rate is proportional to the total stellar mass of the host galaxy and is possibly related to an old progenitor (see also Scannapieco & Bildsten 2005; Mannucci, Della & Panagia 2006). Based on photometric and spectroscopic observations of SN2005hj, Quimby, Hoflich & Wheeler (2007) suggested that there may be two subgroups within the branch normal SNe Ia, produced by two different progenitor channels. Using a sample of 36 events at intermediate redshift ($z = 0.5$), Ellis et al. (2008) reported that rest-frame ultraviolet spectra of SNe Ia have significant variation.

Recent studies with large SNe Ia samples, from low redshift to high redshift, show a significant correlation between SNe Ia properties and their host galaxies. Using a local SNe Ia sample, Kelly et al. (2010) showed that SNe Ia occurring in physically larger, more massive hosts are ∼10 per cent brighter after light-curve correction. Using the third sample of data from the Harvard-Smithsonian Center for Astrophysics (CfA3), Hicken et al. (2009) demonstrated that SNe Ia that appear in Scd/Sd/Irr hosts and E/S0 hosts may arise from different populations (see also Neill et al. 2009). Using Supernova Legacy Survey (SNLS) and other data, Sullivan et al. (2010) showed that SNe Ia properties depend on the global characteristics of their host galaxies. Lampeitl et al. (2010) confirmed the effect of host galaxies on SNe Ia in the Sloan Digital Sky Survey-II (SDSS-II) Supernova (SN) Survey. Also using data from the SDSS-II SN Survey, Smith et al. (2012) found that the rate of SNe Ia per unit stellar mass is much higher in star-forming host galaxies compared to passive host galaxies, and Galbany et al. (2012) suggested that SNe that exploded at large distances from their elliptical hosts tend to have narrower light curves. With SNFactory data, Rigault et al. (2013) found two possible modes of SNe Ia. The first mode is present in all environments, and the second mode is exclusive to locally passive environments, which are intrinsically brighter, and occurs predominately in high-mass hosts. These relations between environment and properties of SNe Ia are used in the cosmological studies to reduce uncertainties in distance moduli (e.g. Rigault et al. 2015; Jones, Riess & Scolnic 2015). Nevertheless, using the SDSS-II SN Survey sample, Wolf et al. (2016) reported that there is no evidence of a significant correlation between Hubble residuals and multiple host galaxy properties, such as host stellar mass and star formation rate.

In this study, we investigate the photometric properties of SNe Ia at intermediate redshift ($z \sim 0.2$), based on the previous study of the photometric properties of 108 nearby ($z \sim 0.1$) SNe Ia in Takanashi, Doi & Yasuda (2008) (hereafter TAK08). We use data obtained by the SDSS-II SN Survey (York et al. 2000; Frieman et al. 2008), which are well calibrated, homogeneous and the first large SNe Ia sample at an intermediate redshift. The SDSS-II SN Survey is a survey of supernovae using the wide-field SDSS 2.5-m telescope (Gunn et al. 2006) and wide-field imaging camera (Gunn et al. 1998) at the Apache Point Observatory (APO) operated by an international collaboration. The SDSS-II SN Survey complements existing ground-based low-redshift (LOTOSS, SNfactory, CSP etc.) and high-redshift (ESSENCE, SNLS) SN search programmes. Through repeated scans of the SDSS southern equatorial stripe (82N and 82S, about 2.5 deg wide by 120 deg long) every other night over the course of three three-month campaigns (2005–2007 September–November), the SDSS-II SN Survey obtained well-measured, densely sampled *u*-, *g*-, *r*-, *i*- and *z*-band light curves (Holtzman et al. 2008; Sako et al. 2014).

Table 1. Type and redshift of the SDSS SNe Ia: SC is a spectroscopically confirmed SN Ia, SP is a spectroscopically probable SN Ia and PP is a photometrically probable SN Ia with spectroscopic redshift of the host galaxy.

Type	Number	Average redshift
All	328	0.17
SC	239	0.16
SP	18	0.17
PP[a]	71	0.18

Note. [a]Selected by Sako et al. (2008).

In this paper, we present the photometric properties of the SDSS SNe Ia parametrized by the multiband stretch method (TAK08). In particular, we focus on the stretch distribution of the SDSS SNe Ia and the relationship between a stretch factor and photometric properties.First, we provide information about the data used in this work (Section 2), and then we describe how we parametrize the multiband light curves (Section 3). We discuss the observational selection biases expected in the SDSS SNe Ia (Section 4), and we show the photometric properties of the SDSS SNe Ia, comparing them with those of nearby SN samples from the literature (Section 5.1). We also examine the properties of host galaxy dust (Section 5.2).

The SNe Ia reported to the International Astronomical Union (IAU) have a SN ID such as SN2005eg. However, there are many SNe Ia (most without a spectroscopic typing configuration) that were not reported to the IAU in the SDSS sample used in this study. We use an SDSS SN ID such as SDSS-SN12345 for the names of those SNe without IAU designations in this paper.

2 PHOTOMETRIC DATA

In this study, we use *u*-, *g*-, *r*-, *i*- and *z*-band (Fukugita et al. 1996; Doi et al. 2010) light curves of 328 SNe Ia in the range $0.05 \leq z < 0.24$[1] obtained by the 2005–2007 SDSS-II SN Survey. As we show in Table 1, the sample of SNe Ia (hereafter the SDSS sample) consists of three groups: (1) spectroscopically confirmed SNe Ia; (2) spectroscopically probable SNe Ia; (3) photometrically probable SNe Ia with host galaxy spectroscopic redshifts. The photometrically probable SNe Ia are identified as SNe Ia based on luminosity, colour and light-curve shapes (see details in Sako et al. 2008). We do not include known peculiar SNe Ia classified by Zheng et al. (2008) in the sample (SN2005js, SN2005gj, SDSS-SN7017 and SN2005hk are excluded). In order to avoid photometric systematic uncertainty, we do not use SNe Ia whose photometry is not based upon the SDSS calibration stars in the same frame. Also, in order to reduce uncertainties in estimating light-curve widths, we do not use SNe Ia that were observed after 5 d from the peak brightness. Because we assigned higher priority to spectroscopic observations of not heavily extinct SNe Ia candidates (Sako et al. 2008, 2014),

[1] In order to reduce the uncertainty of the cross-filter *K*-correction, we use only SNe Ia at this redshift range where we do not to have to change a combination of filters.

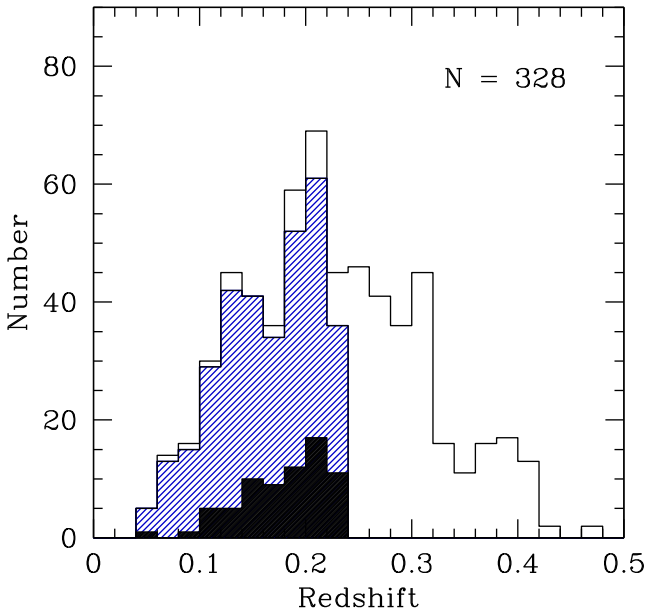

Figure 1. Redshift distribution of all the SNe observed by the SDSS-II Supernova Survey. The shaded histogram shows the 328 SNe used in this work, which we call the SDSS sample. Because we select the SN sample according to the criteria described in Section 2, the number of SNe in the SDSS sample is not as many as in the whole SNe sample, even though at a lower redshift. The filled histogram shows photometrically probable SNe Ia (see Table 1).

spectroscopically observed SNe Ia are biased to blue SNe Ia. To reduce the selection effect, we include photometrically probable SNe Ia in this study. Note that these photometrically probable SNe Ia are not spectroscopically confirmed as SNe Ia.

Fig. 1 shows the redshift distribution of the SDSS sample used in this study. In order to reduce the uncertainty of the cross-filter *K*-correction, we use only SNe Ia at this redshift range where we do not need to change a combination of filters. The redshifts of all SNe in the sample are measured by spectroscopic observations of their host galaxies or SN spectra. The average redshift is $z \sim 0.17$, and about 60 per cent of the sample lies in the range $0.15 < z < 0.24$. Because of insufficient telescope time for spectroscopic observations of faint objects, we did not obtain spectra for many SNe, especially those at higher redshift. We did acquire light curves of many of those missed SNe Ia, but we use only light curves that are classified as having a high probability of being a SN Ia (see Sako et al. 2011).

The photometry of the SNe Ia was mainly obtained by the SDSS camera on the 2.5-m telescope at the APO. The flux of each SN Ia has been measured by Holtzman et al. (2008) with the technique called scene modelling photometry (SMP). SMP does not use a template-subtracted image for photometry. The technique fits all of the individual reduced frames with a model of the galaxy background and the SN, and measures the flux from the model. The model of each image is generated from the sum of a set of stars, a galaxy, a SN and background. As a result, SMP can avoid degrading the point spread function (PSF) and any spatial resampling that leads to correlated noise between pixels. The basic concept is similar to the technique of the SNLS (Astier et al. 2006).

In order to discuss the properties of the SDSS sample, we use the nearby SNe Ia sample (hereafter called the Nearby sample) from TAK08. The Nearby sample includes 108 SNe Ia in the range $z < 0.11$ with *U*-, *B*-, *V*-, *R*- and *I*-band light curves. The light curves were parametrized by the multiband stretch method and the parameters are listed in table 2 of TAK08.

3 ANALYSIS

We applied the multiband stretch method (TAK08) to the light curves in five passbands. This method is a revised stretch method (cf. Perlmutter et al. 1997; Goldhaber et al. 2001) extended to five bands. There are several methods for parametrizing the light-curve shapes of SNe Ia. For example, MLCS (Riess, Press & Kirshner 1996) and SALT2 (Guy et al. 2007) are widely used algorithms. These methods fit parameters of light-curve width and dust extinction to observed light curves at once. The reason that we apply a stretch factor to the *U*, *B*, *V*, *R* and *I* bands independently instead of a common stretch factor such as SALT2 is that we want to investigate the diversity of light-curve shapes independently. We can simply parametrize light-curve shapes and peak brightness without any additional assumptions, such as dust extinction models.

We fit up to 11 parameters to each event: *U*-, *B*-, *V*-, *R*- and *I*-band stretch factors, *U*-, *B*-, *V*-, *R*- and *I*-band peak magnitudes and a time $t_{B\mathrm{max}}$ for maximum light in the *B* band. Only $t_{B\mathrm{max}}$ is common to all passbands, and the remaining 10 parameters are treated equally and independently. The method does not include any dust/colour corrections and has the advantage that we can simply parametrize the light-curve shape and luminosity without any assumptions. We used the *U*-, *B*-, *V*-, *R*- and *I*-band light-curve templates, which are adjusted to coincide with a SN Ia with an $s_{(B)} = 1.0$ SED template (Nugent, Kim & Perlmutter 2002) for the light-curve fitting. We derived absolute magnitudes for the SDSS sample using redshifts under the assumption of the flat ΛCDM model with standard cosmological parameters: $H_0 = 68.5$ km s^{-1} Mpc^{-1}, $\Omega_\mathrm{M} = 0.303$ and $\Omega_\Lambda = 0.697$ from Betoule et al. (2014). We corrected extinction by dust in the Milky Way according to Schlegel, Finkbeiner & Davis (1998). We also corrected the cosmological time dilation. The differences from the analysis in TAK08 are that we need to transform the photometric data from the native SDSS system to the Vega system, and that we must apply cross-filter *K*-corrections to the data. We describe these procedures in the following.

3.1 Magnitude system

The SMP data are provided in the natural system of the SDSS 2.5-m telescope (Doi et al. 2010). We need to transform these *ugriz* data to the Vega system to compare SDSS photometry with *U*-, *B*-, *V*-, *R*- and *I*-band light curves of the Nearby sample. We transformed the data in the following way.

First, the native SDSS system was transformed into the AB system (Sako et al. 2014):

$$u(\mathrm{AB}) = u(\mathrm{SDSS}) - 0.0679;$$
$$g(\mathrm{AB}) = g(\mathrm{SDSS}) + 0.0203;$$
$$r(\mathrm{AB}) = r(\mathrm{SDSS}) + 0.0049;$$
$$i(\mathrm{AB}) = i(\mathrm{SDSS}) + 0.0178;$$
$$z(\mathrm{AB}) = z(\mathrm{SDSS}) + 0.0102.$$

Next, the AB system was transformed into the Vega system. To adjust zero points of the AB system and the Vega system, the *u*-, *g*-, *r*-, *i*- and *z*-band magnitudes of Vega in the AB system (Table 2) were added as follows:

$$u(\mathrm{Vega}) = u(\mathrm{AB}) - u(\mathrm{AB})_\mathrm{Vega}$$
$$g(\mathrm{Vega}) = g(\mathrm{AB}) - g(\mathrm{AB})_\mathrm{Vega}$$

Table 2. Synthetic AB magnitude of Vega in the SDSS filters, calculated from the STSDAS v3.3 synphot Vega spectrum assuming $V = +0.03$.

u	g	r	i	z
0.951	−0.080	0.169	0.389	0.556

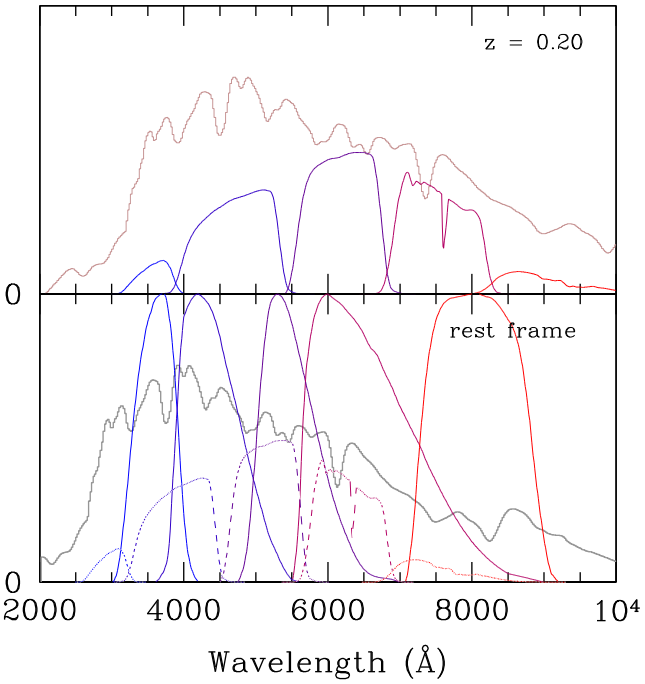

Figure 2. In the top panel, we show u-, g-, r-, i- and z-band response curves (including atmosphere) and a SN Ia spectrum at maximum, which is shifted to $z = 0.2$. In the bottom panel, we show U-, B-, V-, R- and I-band responses as solid lines, shifted u-, g-, r-, i- and z-band responses at $z = 0.2$ as dashed lines and a rest-frame SN Ia spectrum at maximum.

$$r(\mathrm{Vega}) = r(\mathrm{AB}) - r(\mathrm{AB})_{\mathrm{Vega}}$$
$$i(\mathrm{Vega}) = i(\mathrm{AB}) - i(\mathrm{AB})_{\mathrm{Vega}}$$
$$z(\mathrm{Vega}) = z(\mathrm{AB}) - z(\mathrm{AB})_{\mathrm{Vega}}.$$

At the end of this procedure, we have transformed the u-, g-, r-, i- and z-band magnitudes of the SDSS SNe into the Vega system.

3.2 Cross-filter *K*-correction

The next step is to apply K-corrections to transform observed u-, g-, r-, i- and z-band magnitudes to U-, B-, V-, R- and I-band magnitudes (see Fig. 2). We have to choose an appropriate filter combination for each cross-filter K-correction as a function of redshift. In this study, we transformed $(u, g, r, i, z) \rightarrow (U, B, V, R, I)$ in the range $0.05 \leq z < 0.24$.

The cross-filter K-correction was applied according to Kim, Goobar & Perlmutter (1996). We use the spectrum of Hsiao et al. (2007) for the K-correction. Ideally, we should apply a spectrum template based on the proper type of each SN Ia (e.g. SN1991T-like, SN1991bg-like) for K-corrections, but we applied Hsiao's template all SNe Ia. The template is warped to fit the observed *ugriz* photometry. We use the standard galactic extinction curve (Cardelli, Clayton & Mathis 1989) for warping.

Because we have calibrated the flux with only the cross-filter K-correction, we should also apply the stretch K-correction. As we have noted above, we chose the appropriate filter combination for the cross-filter K-correction as a function of redshift, but the K-corrected bandpass of the observed band is not the same as that of the rest-frame B band. We should correct the difference of the stretch factors because of the different bandpass. We use the relations between $s_{(B)}$ and the stretch factors of other bands derived from the Nearby SNe Ia (Table 3) for the stretch K-correction. Based on these relations, we calculated the size of the stretch K-correction by interpolating stretch factors of different two bands. Fig. 3 shows the size of the stretch corrections of the SDSS SNe Ia versus redshift. We show the typical size of the stretch correction of the SN Ia with $s_{(B)} = 1.0$ as a solid line. The correction becomes smallest at the redshift where the K-corrected bandpass of the observed band agrees well with that of the rest-frame B band. For the SDSS SNe Ia, the correction reaches a maximum of 5 per cent in the range $0.05 \leq z < 0.24$.

Table 3. Relations between B-band stretch factor and stretch factors in the U and V bands of the Nearby SNe Ia from TAK08.

Relation	rms	Number
${}^{s}_{(U)} = (0.95 \pm 0.02) \times {}^{s}_{(B)} + (0.16 \pm 0.02)$	0.09	75
${}^{s}_{(V)} = (0.88 \pm 0.01) \times {}^{s}_{(B)} + (0.16 \pm 0.01)$	0.08	92

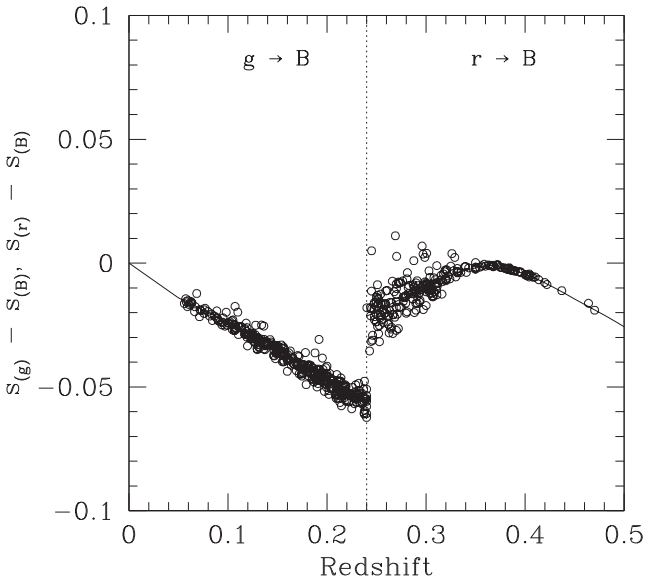

Figure 3. Stretch corrections of each SN Ia versus redshift. We need to correct the g-band and r-band stretch factor to the rest-frame B-band stretch factor (g-band in the range $z \leq 0.24$ and r-band in the range $0.24 < z < 0.50$) as the stretch factors of a SN Ia in different filter bands are not same. The solid line shows the size of stretch correction of SN Ia ($s_{(B)} = 1.0$). See text for description.

3.3 Uncertainty of the analysis

We now consider the uncertainties in our analysis. The uncertainties are divided into three components: uncertainty due to the light-curve fitting (including observational photometric uncertainties), uncertainty due to the K-correction and uncertainty due to the cosmological parameters adopted.

We estimated the uncertainty due to the light-curve fitting with Monte Carlo simulations. We created artificial light curves from the light-curve template based on the observed dates and photometric

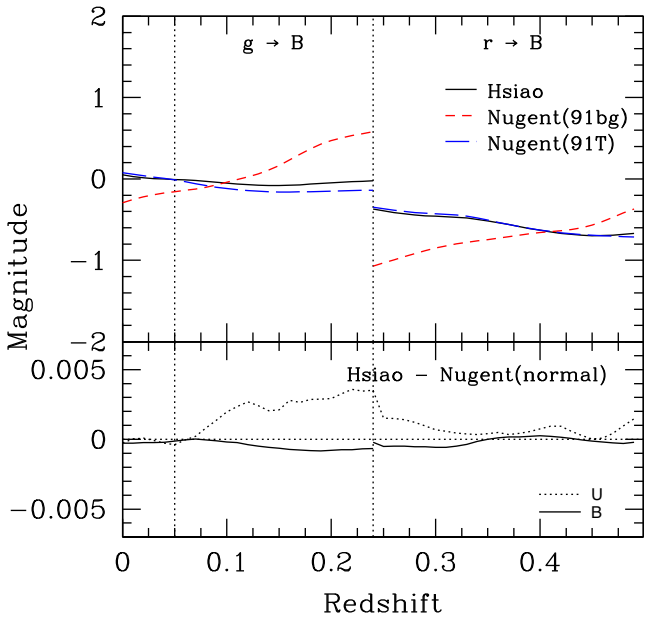

Figure 4. In the top panel, we show the amount of *K*-correction ($g \rightarrow B$, $r \rightarrow B$) at *B*-band maximum calculated from three different types of SN Ia template versus redshift. The black solid line is calculated from Hsiao's template (corresponding to Nugent's normal template), the short-dashed red line is calculated from Nugent's SN1991bg-like template and the long-dashed red line is calculated from Nugent's SN1991T-like template. In the bottom panel, we show the difference between *K*-corrections calculated from Hsiao's template and Nugent's Branch Normal template in the *U* and *B* bands versus redshift. Vertical dotted lines denote the border of band combinations for the *K*-correction.

uncertainties of each epoch. We measured the dispersion of each fitting parameter (luminosity, stretch factor and time) and estimated the size of the uncertainties. The typical uncertainties in estimating luminosity at $z = 0.2$ are ∼0.4 mag in the *U* band, ∼0.06 mag in the *B*, *V* and *R* bands and ∼0.2 mag in the *I* band. The typical uncertainties in estimating stretch factors at $z = 0.2$ are ∼0.3 in the *U* band, ∼0.05 in the *B* and *V* bands, ∼0.1 in the *R*band and ∼0.3 in the *I* band.

It is difficult to estimate the uncertainty due to the *K*-correction. As described above, we applied Hsiao's template to all SNe Ia in our sample; some SNe in our sample might include SNe Ia that have spectra that differ from Hsiao's template. If one particular SN Ia has a spectrum that differs greatly from Hsiao's template, such as that of SN1991T or SN1991bg, we might significantly overestimate or underestimate the size of the *K*-correction. For example, we show the value of the *K*-correction at the *B*-band maximum versus redshift in the top panel of Fig. 4. As is clear in the figure, the difference is significantly larger than the uncertainties due to light-curve fitting.

If the SN Ia has a spectrum similar to that of Hsiao's template, then the typical uncertainties in the *K*-correction are 0.01–0.02 mag in the range $z < 1.0$ from the SNLS study (Foley, Filippenko & Jha 2008b). We also compared the difference between Hsiao's template and Nugent's template Branch Normal (in the bottom panel of Fig. 4), and we have confirmed that the difference is negligible (the size is only <0.005 mag in the *U* and *B* bands).

The uncertainty due to the cosmological parameters also affects our estimation of distance modulus (absolute magnitude). If H_0 moves 1σ (± 1.27 km s^{-1} Mpc^{-1}; Betoule et al. 2014), the distance modulus changes by 0.04 mag. Adopting a slightly different value for H_0 only shifts the zero point of the absolute magnitude, and it does not affect the conclusions in this study. A change of 1σ in Ω_m and Ω_Λ is equivalent to only 0.002 mag of distance modulus at $z = 0.2$. Note that the uncertainty is negligible for the comparison of samples with the same redshift, but it is important for the comparison of samples with different redshifts.

Table 4. Typical uncertainty in estimating luminosity and stretch factors at $z = 0.2$.

	σ_{M_B}	SF
Light-curve fitting[a]	0.06	0.05
K-correction[b]	0.02	–
Cosmological parameters	0.002	–
Redshift estimation	0.01	–
Total	0.06	0.05

Notes. [a]Including photometric uncertainties of each epoch. [b]Branch Normal SNe Ia only (Foley et al. 2008a).

Any uncertainty in the redshift of an event creates a corresponding uncertainty in its distance modulus. The redshifts of all SNe Ia used in this study were measured by a host galaxy spectrum or a SN spectrum, with a typical uncertainty in redshift of 0.001; this corresponds to an uncertainty of 0.01 mag at $z = 0.2$.

The main component of uncertainty is due to light-curve fitting (see Table 4). In the following discussion, the uncertainties of each parameter include all of the uncertainties.

4 OBSERVATIONAL BIAS OF THE SDSS SAMPLE

In this section, we discuss the observational biases of the SDSS sample used in this study.

4.1 Selection bias of the SDSS sample

The most important case of selection biases in the SDSS sample is a result of the detection limit of the SDSS 2.5-m photometry in which the candidates are identified (see Fig. 5). The signal-to-noise ratio (S/N) threshold for object detection is ∼3.5, in typical conditions, corresponding to $g \sim 23.2$, $r \sim 22.8$ and $i \sim 21.2$ mag in the AB system (Dilday et al. 2008). From Monte Carlo simulations with artificial SNe, Dilday et al. (2008) showed that the survey efficiency is 100 per cent for candidates whose *g*-band maximum brightness is brighter than ∼21.2 mag.

Another aspect is the bias resulting from the SN search strategy, especially spectroscopic target selection (see Sako et al. 2008). Because the survey typically found 10 SN candidates per night, they could not all be observed spectroscopically. We chose targets for spectroscopic observations based on their probability of being SNe Ia. The likelihood was calculated from *g*-, *r*- and *i*-band light-curve fitting with four parameters: z, $A_{V\mathrm{sdss}}$, $T_{\max}$ and a template. Here, $A_{V\mathrm{sdss}}$ is the host galaxy extinction in the *V* band under the assumption that $R_V = 3.1$, $T_{\max}$ is the time of the rest-frame *B*-band maximum light and the template is taken from a set of seven light curves, of SNe Ia (normal, SN1991T-like and SN1991bg-like), Ib, Ic, II-P and II-L SNe.

We searched for best-fitting parameters for each candidate, and ranked them by the probability of being SNe Ia. Highly extinct SNe (beyond $A_V = 1.0$ for the 2005 run and $A_V = 3.0$ for the 2006 and 2007 runs) are removed from the SDSS sample, but the number of those missed SNe Ia may be very small;

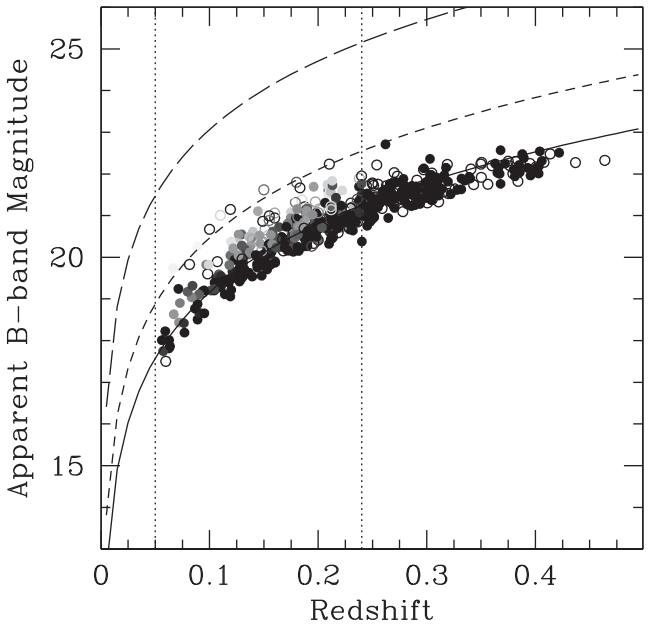

Figure 5. Apparent peak *B*-band magnitude versus redshift of the SNe Ia observed by the SDSS-II SN Survey with uncertainties less than 0.2 mag. Filled symbols are spectroscopically confirmed SNe Ia and open symbols are spectroscopically or photometrically probable SNe Ia. The solid line denotes the typical luminosity of SN Ia, −19.2 + distance modulus. The dashed lines denote the limits of host galaxy dust extinction parameter A_V (we transformed A_V to A_B in this figure); we set the value to 1.0 mag for the 2005 survey (short-dashed line) and to 3.0 mag for the 2006–2007 survey (long-dashed line). SNe plotted between dotted lines are the SDSS sample. The darker symbols are the bluer SNe Ia and the lighter symbols are the redder SNe Ia.

Sako et al. (2008) reported that only two SNe are missed in 2005 run (see also Fig. 5). Many SNe Ia with lower priorities were undoubtedly lost from spectroscopically confirmed SNe Ia subsamples, especially if the colour of the SN Ia differs from the template or the host galaxy extinction law differs from the galactic extinction law. In fact, the average $(M_B - M_V)_{\max}$ of spectroscopically confirmed SNe Ia is 0.05, which is bluer than that of spectroscopically or photometrically probable SNe Ia – average $(M_B - M_V)_{\max}$ = 0.09. In order to reduce the selection bias due to spectroscopic target selection, the SDSS sample used in this paper includes not only spectroscopically confirmed SNe Ia but also spectroscopically or photometrically probable SNe Ia.

4.2 Contamination by other types of SNe

As discussed in Section 2, we added spectroscopically or photometrically probable SNe Ia to the SDSS sample in order to reduce the biases described above and to preserve the diversity of the sample, as spectroscopically confirmed SNe Ia are strongly biased (Sako et al. 2011). However, the incorporation of photometrically probable SNe Ia may introduce contamination by other types of SNe. According to spectroscopic observations of SN Ia candidates that correspond to photometrically probable SNe Ia, the probability of misidentification is about 10 per cent (Dilday et al. 2008). Because the SN candidates were selected based only on photometry at early phases, the probability of misidentification would be smaller than 10 per cent for photometrically probable SNe Ia with late epoch observations. Sako et al. (2011) estimates that the purity of photometrically probable SNe Ia is ∼91 per cent and the contamination by other types of SNe is ∼6 per cent. So, there must be less than seven of those misidentified SNe in the SDSS sample (we have 71 photometrically probable SNe Ia at the redshift range).

5 RESULTS

5.1 Photometric properties of the SDSS sample

As we have already described, we use 328 SNe Ia in the range $0.05 \leq z < 0.24$. At this redshift range, the bluer SNe Ia are almost complete, but the redder SNe Ia are not complete (see Fig. 5). However, the selection bias due to the redshift cut-off is not important for the following discussion.

Because of poor *u*- and *z*-band photometry relative to the *g*, *r* and *i* bands, we do not use stretch factors and peak magnitudes of the *u* and *z* bands in this study (the *u* band corresponds to the *U* band and the *z* band corresponds to the *I* band in the range $z < 0.24$). Also, the sample does not include SNe with large photometric uncertainties (>20 per cent). All the parameters of the 328 SNe Ia are given in the table included online as Supporting Information (partly given in Table 5).

5.1.1 Stretch factor distribution

The stretch factor is one of the simplest parameters reflecting the intrinsic properties of SNe Ia among the parameters derived from light-curve fitting, as stretch factors are not affected by the host galaxy dust. In the lower-right panel of Fig. 6, we show the distribution of the *B*-band stretch factor of the SDSS sample. In this figure, we also show the stretch distributions of the Nearby SNe Ia used in TAK08, in which three major data sets were identified:

Table 5. Sample of the fitting parameters of the 328 intermediate-redshift SDSS SNe Ia. Peak magnitudes are shown in the Vega system. The redshift of the SN Ia is published in Sako et al. (2011). Complete data are provided as Supporting Information online.

SDSS-SNID	SN name	Redshift	$s_{(B)}$	M_B	M_V	M_R	M_I
762	2005eg	0.19	1.14(0.05)	−18.86(0.07)	−18.89(0.03)	−18.88(0.05)	−18.58(0.32)
1032	2005ez	0.13	0.74(0.03)	−18.42(0.11)	−18.49(0.05)	−18.62(0.04)	−18.77(0.16)
1241	2005ff	0.09	0.93(0.01)	−18.83(0.04)	−18.91(0.03)	−18.93(0.03)	−18.78(0.07)
1371	2005fh	0.12	1.09(0.02)	−19.47(0.04)	−19.38(0.03)	−19.35(0.04)	−19.17(0.06)
1395	–	0.19	1.00(0.06)	−18.77(0.10)	−18.75(0.06)	−18.92(0.06)	−18.73(0.16)
1415	–	0.21	1.12(0.08)	−18.51(0.07)	−18.78(0.05)	−18.79(0.06)	−19.06(0.20)
1525	–	0.11	1.73(0.08)	−18.41(0.05)	−18.28(0.02)	−18.65(0.03)	−18.48(0.03)
1595	–	0.21	1.00(0.05)	−19.10(0.07)	−19.05(0.06)	−19.10(0.05)	−18.91(0.17)
1740	–	0.17	0.94(0.05)	−18.80(0.08)	−18.79(0.03)	−18.86(0.04)	−18.79(0.16)
1794	2005fj	0.14	1.21(0.06)	−18.85(0.05)	−18.87(0.03)	−18.84(0.03)	−18.52(0.19

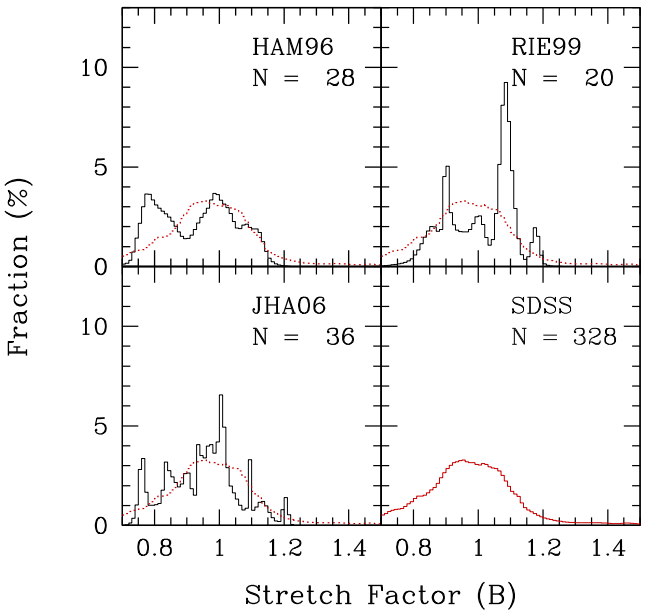

Figure 6. Distribution of *B*-band stretch factors of the Nearby SNe Ia (TAK08) found by three different groups (HAM96, RIE99 and JHA06). The black line is the Nearby SNe Ia sample found by each group, the red line is the distribution of the SDSS SNe Ia in the range $0.05 \leq z < 0.24$ and the red dotted line is the same distribution of the SDSS sample. The histograms are made from *B*-band stretch factors, which are smoothed by estimated uncertainties.

28 SNe Ia from Hamuy et al. (1996a), hereafter HAM96; 20 SNe Ia from Riess et al. (1999), hereafter RIE99; 36 SNe Ia from Jha et al. (2006), hereafter JHA06.

The SNe Ia shown in RIE99 and JHA06 were not discovered in a systematic SN search programme. Their SNe Ia were selected from the IAU's Central Bureau for Astronomical Telegrams (CBAT). The SNe Ia shown in HAM96 were discovered by the CALAN/TOLOLO Supernova Search (Hamuy et al. 1993), which is a repeated scan SN survey of galaxy clusters that includes many early-type galaxies. This may result in an excess of events with a lower stretch value in the HAM96 sample as early-type galaxies tend to host lower-stretch SNe Ia (cf. Howell 2001; van den Bergh, Li & Filippenko 2005). The stretch distributions of HAM96 shown in Fig. 6 seem to have more SNe Ia with small stretch values than those in RIE99 and JHA06; recall that SNe with small stretch values are expected to be fainter than average SNe Ia. This difference may be caused by observational selection biases, as the samples composed of SNe Ia reported in CBAT are expected to include fewer less-luminous SNe Ia with narrower light curves.

In order to compare the photometric properties of the SDSS SNe with different stretch factors, we classified the SDSS sample into three subsamples as follows: narrow, $s_{(B)} \leq 0.9$; medium, $0.9 < s_{(B)} \leq 1.1$; broad, $s_{(B)} > 1.1$.

5.1.2 *Stretch–magnitude relation*

We compared the stretch–magnitude relations derived from the bluest SNe [$-0.14 \leq (M_B - M_V)_{\max} \leq -0.10$] of the Nearby and SDSS samples (Table 6), which are expected to be almost free from dust extinction. The slopes of the *B*-band stretch–magnitude relations of the SDSS sample and the Nearby sample are consistent within the uncertainties, although those of their *V*-band stretch–magnitude relations are not consistent.

Table 6. Relations of *B*-band stretch factor and *B*- and *V*-band magnitudes of the bluest SNe. The relations of the Nearby SNe are from TAK08.

Relation	rms (mag)	No.
Nearby sample		
$M_B = (2.28 \pm 0.42) \times s_{(B)}^{-1} - (21.49 \pm 0.41)$	0.17	21
$M_V = (2.58 \pm 0.38) \times s_{(B)}^{-1} - (21.67 \pm 0.38)$	0.20	21
SDSS sample		
$M_B = (1.71 \pm 0.31) \times s_{(B)}^{-1} - (20.73 \pm 0.31)$	0.16	15
$M_V = (1.59 \pm 0.26) \times s_{(B)}^{-1} - (20.51 \pm 0.25)$	0.16	15

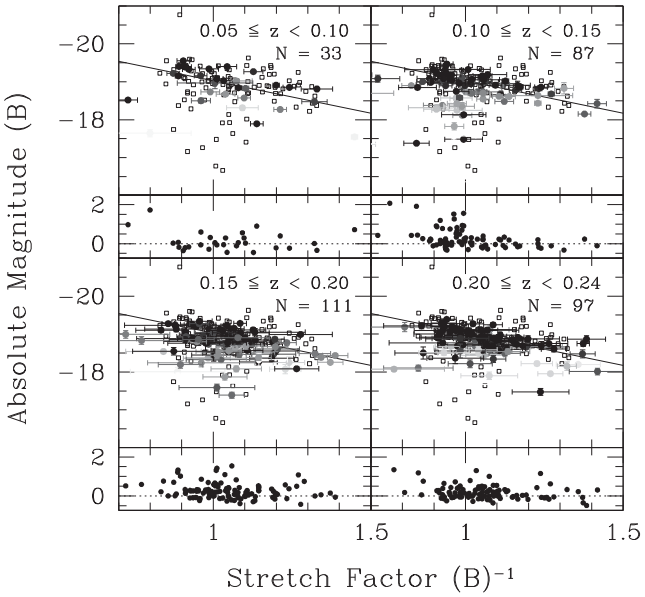

Figure 7. Relation between the inverse *B*-band stretch factor and the *B*-band peak magnitude (upper panels) and ΔM_B (lower panels) at different redshift bins. In the upper panels, circles are the SDSS sample and open squares are the Nearby sample. The thickness of the circles is related to $(M_B - M_V)_{\max}$, the darker circles are the bluer SNe Ia and the lighter circles are the redder SNe Ia (as in Fig. 5). The solid line denotes the relation between the inverse *B*-band stretch factor and the *B*-band magnitude derived from the SDSS sample. In the lower panels, positive ΔM_B indicates that a photometric point is below the regression line.

Fig. 7 shows the *B*-band stretch–magnitude relation in different redshift bins; 90 per cent of the SDSS sample is under the stretch–magnitude relation derived from the bluest SDSS sample ($M_B = 1.71 \times s_{(B)}^{-1} - 20.73$).[2]

We define the *B*-band residual (hereafter ΔM_B) as $\Delta M_B = M_B - (1.71 \times s_{(B)}^{-1} - 20.73)$, which is the difference between M_B estimated from photometry and intrinsic luminosity estimated from the stretch–magnitude relation of the SDSS sample. Fig. 8 shows the histogram of ΔM_B of the SDSS sample using the stretch–magnitude relation derived from the SDSS sample. Host galaxy dust extinction is one of the possible explanations of the tails towards large ΔM_B.

5.1.3 *Stretch–colour relation*

In order to discuss the nature of the SNe Ia colour and variety of host galaxy dust extinction in Section 6, we use $M_B - M_V$ colour at the

[2] We use the inverse *B*-band stretch factor in Fig. 7 for comparison with fig. 16 in TAK08.

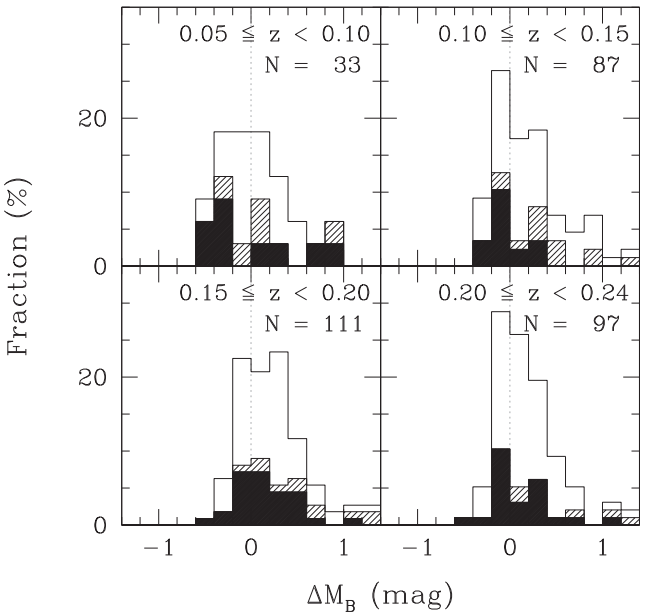

Figure 8. Histogram of ΔM_B of the SDSS sample at each redshift bin. The shaded histograms show the broad SNe Ia, the filled histograms show the narrow SNe Ia and the remaining histograms are the normal SNe Ia.

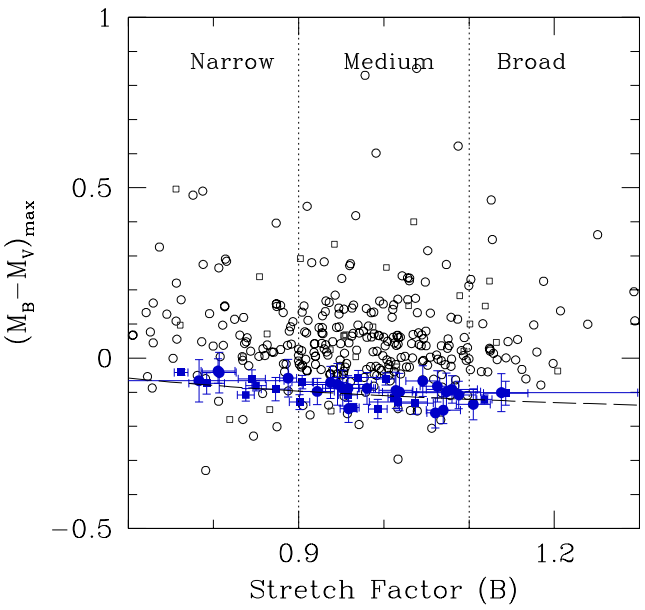

Figure 9. A relation between the B-band stretch factor and $(M_B - M_V)_{\max}$ of the Nearby and SDSS samples. The squares are the Nearby SNe Ia and the circles are the SDSS SNe Ia, in which blue filled symbols are the BV-selected SNe Ia with a smaller photometric uncertainty. The diagonal dashed line shows the relation between the B-band stretch factor and $(M_B - M_V)_{\max}$ of bluest sample of the SDSS SNe Ia used for the definition of SNCE.

B-band maximum date because the B and V bands are the bands with the least dispersion among optical passbands (James et al. 2006). Fig. 9 shows the colour distribution of the SDSS sample; 93 per cent of the SNe are above the stretch–colour relation derived from the SDSS sample.

We define the supernova colour excess (hereafter SNCE) as SNCE $= (M_B - M_V)_{\max} - (0.12 \times s_{(B)}^{-1} - 0.22)$, which is the difference between $(M_B - M_V)_{\max}$ estimated from photometry and intrinsic colour estimated from the stretch–magnitude relations of the SDSS sample (Table 6).

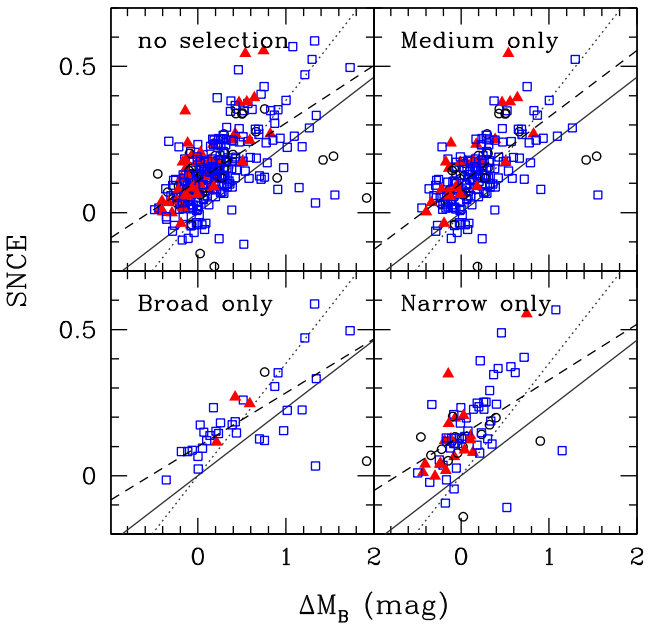

Figure 10. Relations between ΔM_B from the stretch–magnitude relation and SNCE from the stretch–colour relation of the SDSS SNe Ia. The top-left panel shows all of the SDSS sample and the other panels show subsamples (medium, broad and narrow, respectively). The blue open squares show the SNe Ia that appeared in blue host galaxies, the red filled triangles show the SNe Ia that appeared in red host galaxies and the black open circles show the SNe Ia that appeared in the intermediate-colour galaxies. Average estimation uncertainties are 0.06 mag for ΔM_B and 0.08 mag for SNCE. The solid lines denote the conversion factor of standard Galactic extinction ($R_V = 3.3$), the dotted lines denote a smaller conversion factor ($R_V = 2.0$) and the dashed lines denote the best linear fit. See also Table 7.

5.2 Photometric properties of host galaxies

5.2.1 *Extinction law of host galaxy dust*

It is important to correct for dust extinction in the host galaxy before performing the distance estimation using SNe Ia. In particular, we must know the shape of the extinction curve (colour–colour relation) and the zero point of the extinction curve (magnitude–colour relation).

Because ΔM_B and SNCE are possibly due to host galaxy dust extinction, the ΔM_B–SNCE relation gives us a clue to understanding the properties of host galaxy dust. Fig. 10 shows the ΔM_B–SNCE relation of the SDSS samples, which include medium, broad and narrow SNe Ia subsamples. In Section 6, we discuss the possibility that there are different stretch–colour relations for the SNe Ia with different stretch factors. The relations and conversion factors we derive are shown in Table 7.

5.2.2 *Relations between SNe Ia and host galaxy colour*

We investigated relationships between the photometric properties of SNe Ia and their host galaxy types. Using galaxies brighter than $g = 21$ in the SDSS imaging data, Strateva et al. (2001) found that 90 per cent of spectroscopically classified late-type galaxies have colour bluer than $u - r = 2.5$ and they found no examples of spectroscopically classified early-type galaxies with colour bluer

Table 7. Relations between ΔM_B and SNCE of each subsample. R_V is the conversion factor of the V band translated from R_B. See also Fig. 10.

Sample	Relation	R_V	Number
Broad	$(0.18 \pm 0.01) \times \Delta M_B + (0.10 \pm 0.01)$	$4.3^{+0.2}_{-0.3}$	39
(Blue host only)	$(0.21 \pm 0.01) \times \Delta M_B + (0.09 \pm 0.01)$	$3.7^{+0.1}_{-0.2}$	34
Medium	$(0.23 \pm 0.01) \times \Delta M_B + (0.10 \pm 0.01)$	$3.3^{+0.2}_{-0.1}$	208
(Blue host only)	$(0.21 \pm 0.02) \times \Delta M_B + (0.09 \pm 0.01)$	$3.7^{+0.3}_{-0.4}$	154
(Red host only)	$(0.38 \pm 0.03) \times \Delta M_B + (0.14 \pm 0.01)$	$2.0^{+0.2}_{-0.1}$	28
Narrow	$(0.19 \pm 0.03) \times \Delta M_B + (0.14 \pm 0.01)$	$4.0^{+0.8}_{-0.5}$	81
(Blue host only)	$(0.34 \pm 0.04) \times \Delta M_B + (0.14 \pm 0.01)$	$2.3^{+0.3}_{-0.3}$	49
(Red host only)	$(0.28 \pm 0.13) \times \Delta M_B + (0.14 \pm 0.03)$	$2.8^{+2.3}_{-0.9}$	18
All	$(0.15 \pm 0.06) \times \Delta M_B + (0.12 \pm 0.04)$	$5.1^{+3.4}_{-1.4}$	328

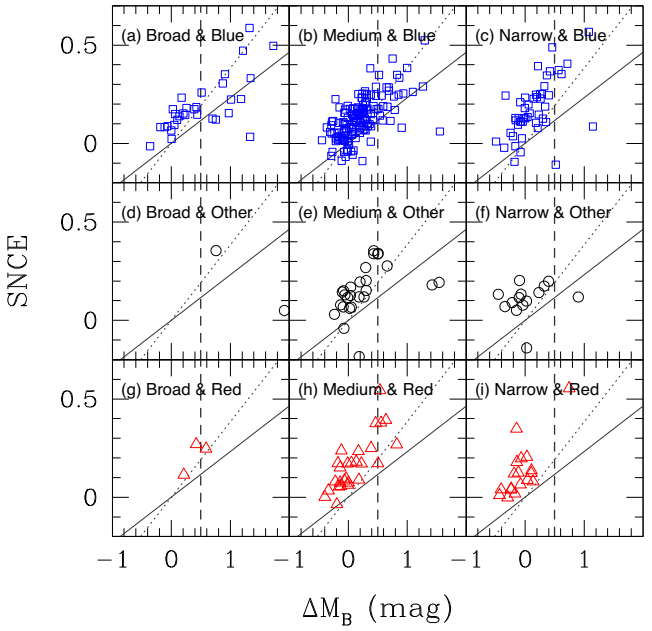

Figure 11. Subsets of the relation between ΔM_B and SNCE of the SDSS SNe Ia. The blue open squares show the SNe Ia that appeared in blue host galaxies (a, b and c), the black open circles show the SNe Ia that appeared in the intermediate-colour galaxies (d, e and f) and the red open triangles show the SNe Ia that appeared in red host galaxies (g, h and i). The left side of the dashed line is sample B (see Table 8). They are also divided into three subgroups: broad, medium and narrow. The solid line is the conversion factor of standard Galactic extinction ($R_V = 3.3$) and the dotted line denotes a smaller conversion factor ($R_V = 2.0$).

than $u - r = 2.05$. Based on the $u - r$ colour of the host galaxy, we classified the SDSS SNe Ia into three subgroups as follows: blue host, $u - r < 2.0$ corresponding to late types (Sb, Sc and Irr); red host, $u - r > 2.5$ corresponding to early types (E/S0 and Sa); intermediate colour, $2.0 \leq u - r \leq 2.5$. We show the relations between SNe Ia and host galaxy type in Table 7 and Figs 10 and 11.

Blanton & Berlind (2007) and Skibba et al. (2009) show a different colour cut, $g - r = 0.8 - 0.03 \times (M_r + 20)$ for separating the red sequence and blue cloud of galaxies. However, this colour cut is similar to the colour cut proposed by Strateva et al. (2001) and the latter is a more strict colour cut for selecting early-type galaxies. We use the colour cut proposed by Strateva et al. (2001) in this study. The specific star formation rates (sSFRs) of 125 blue host galaxies and 16 red host galaxies have been published by Wolf et al. (2016).

Table 8. Dispersion of residuals around the relations of ΔM_B and SNCE of each subsample. Sample A is all of the SNe of the subgroup, and sample B is the SNe with $\Delta M_B < 0.5$ mag. See also Fig. 11.

Sample		Red host		Blue host		All	
		σ (mag)	Number	σ (mag)	Number	σ (mag)	Number
Broad	A	–	3	0.19	34	0.19	39
	B	–	2	0.04	18	0.04	20
Medium	A	0.08	28	0.11	154	0.11	208
	B	0.06	22	0.07	126	0.08	169
Narrow	A	0.09	18	0.15	49	0.12	81
	B	0.05[a]	16	0.12	43	0.11	73
Total			49		237		328

Note. [a]One outlier is excluded because the SN has a dispersion larger than 5σ.

The average sSFR of the blue host galaxies is -9.78 $M_\odot$ yr^{-1} and that of the red host galaxies is -11.34 $M_\odot$ yr^{-1}. This result supports the idea that the blue host galaxies correspond to late types and the red host galaxies correspond to early types.

Fig. 10 shows that the SNe Ia that appeared in the red host galaxies have a smaller dispersion in SNCE around the best-fitting relation than the SNe Ia that appeared in the blue host galaxies (see also Table 8). In addition, the medium and narrow SNe Ia that appeared in the red host galaxies have smaller ΔM_B than the SNe Ia that appeared in the blue host galaxies. Table 8 also shows that the dispersion in SNCE around the best-fitting relation is smaller in each SN Ia subsample with $\Delta M_B < 0.5$ mag (Table 8, sample B).

6 DISCUSSION

Because the SDSS SN Ia sample is more homogeneous than any other large sample of SNe Ia from surveys at lower redshift, the photometric properties derived might give us a clue to understanding the nature of spectroscopically normal SNe Ia. Hence, it is worth looking into the photometric properties of SDSS SNe Ia in detail.

In particular, the ΔM_B–SNCE relation is quite interesting (see Fig. 10). The dispersion around the ΔM_B–SNCE relation (Table 8) might be consistent with the uncertainties (see Table 4) under the two assumptions that (i) peak luminosities and colours are the same for all SNe Ia after the stretch correction, and (ii) extinction laws of dust in host galaxies are the same. However, the dispersion of the medium sample (0.11 mag) appears to be larger than the typical uncertainty (σ in colour is 0.08 mag at $z = 0.2$). This implies that the assumptions may be too simplified. We now discuss the possible

Table 9. Host galaxies of SNe Ia with $\Delta M_B \geq 0.5$, which are excluded from sample B in Table 8. Morphology is determined by eye inspections and spectral type is determined by the SDSS-III Baryon Oscillation Spectroscopic Survey (BOSS).

ΔM_B	SDSS-SNID	SN name	Host name	Morphology	Spectral type
0.51	13224	–	SDSS J030958.79–001444.8	?	N/A
0.54	20376	–	SDSS J211734.92–003126.3	?	N/A
0.56	12778	2007re	SDSS J210958.95+002430.9	Spiral	Star-forming
0.64	1415	–	SDSS J002425.55+003556.4	Spiral	Broad-line
0.82	3488	–	SDSS J205413.25–010037.2	?	N/A
2.54	19003	2007mp	2MASX J21163594–0046133	Spiral	AGN Broad-line

diversity of the photometric properties of SNe Ia and the properties of dust extinction in their host galaxies.

6.1 Diversity of photometric properties of SNe Ia

Table 8 shows that the SNe Ia that appeared in the red host galaxies tend to have a narrower light-curve width (3 out of 39 SNe of the broad sample, 28 out of 208 SNe of the medium sample and 18 out of 81 SNe of the narrow sample are red host SNe; see also the ratio of red filled triangles to other symbols in Fig. 10). Because many red host galaxies are early-type galaxies, the tendency for red host SNe Ia to have a narrower light-curve width is consistent with previous studies (cf. Hamuy et al. 1996b, 2000; Howell 2001; van den Bergh et al. 2005; Sullivan et al. 2006). However, the SNe Ia that appeared in blue host galaxies have a variety of light-curve widths (34 out of 39 SNe of the broad sample, 154 out of 208 SNe of the medium sample and 49 out of 81 SNe of the narrow sample are blue host SNe; see also the ratio of blue open squares to other symbols in Fig. 10).

These observational results can be explained by postulating that the progenitors of SNe Ia that appeared in red host galaxies are members of an old stellar population, but those of SNe Ia that appeared in blue host galaxies may belong to both old and young stellar populations. However, there are six medium SNe Ia that have large ΔM_B although they appeared in red host galaxies (see the top-right panel of Fig. 10). This can be explained if those red host galaxies are dusty red galaxies with large extinction. In fact, Strateva et al. (2001) reported that about 10 per cent (20 out of 210) of late-type galaxies have a colour of $u - r > 2.5$. Table 9 shows that some of those red host galaxies may be dusty red late-type galaxies.

The interpretation that there are two types of SNe Ia with different photometric properties, originating in young and old stellar populations, is consistent with the idea that there are two varieties of SNe Ia, called tardy and prompt (Mannucci et al. 2005). The SNe Ia that appear in red host galaxies are all tardy SNe Ia and the SNe Ia that appear in blue host galaxies are both tardy and prompt SNe Ia. Based on this idea, we can estimate the intrinsic dispersions of the tardy and prompt SNe Ia on the ΔM_B–SNCE plane. In Table 8, the B samples of the red host narrow and medium samples are expected to be pure samples of tardy SNe Ia and the B sample of blue host broad sample is prompt SNe Ia. These dispersions are 0.04–0.06 mag, and the values are smaller than those of the B samples of the blue host medium (0.07 mag) and narrow (0.12 mag) SNe Ia, which are expected to be a mixture of tardy and prompt SNe Ia. This result supports the original idea that there are two distinct populations (tardy and prompt), as proposed by Mannucci et al. (2005).

Fig. 12 shows the distributions of SNCE residuals from the regression line of the ΔM_B–SNCE plane of the medium SNe Ia. The result of the Kolmogorov–Smirnov test shows that the distributions

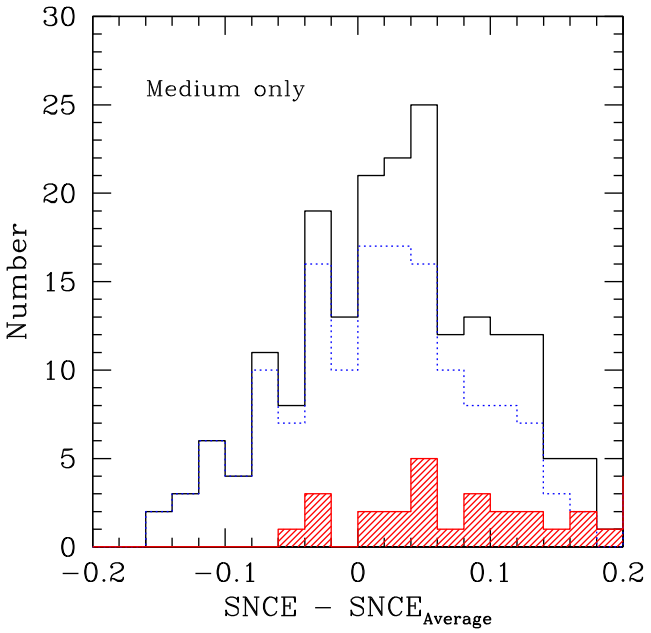

Figure 12. Distributions of colour residuals from the average SNCE (dashed line in Fig. 10) of the medium SNe Ia. The histogram with a dotted blue line shows the blue host SNe Ia, the shaded histogram with a red line shows the red host SNe Ia and the histogram with a solid black line shows all of the medium SNe Ia. Averages of colour residuals are 0.01 mag for the blue host SNe Ia and 0.07 mag for the red host SNe Ia.

of the medium SNe Ia that appeared in the blue host and red host galaxies are different, at a significance level of 99.9 per cent. Averages of colour residuals are 0.01 mag for blue host SNe Ia and 0.07 mag for red host SNe Ia. The colour offset (i.e. tardy SNe are redder and prompt SNe are bluer) can be explained by the idea of two types of SNe Ia with different intrinsic colour. These results support the possibility that there are two different populations of SNe Ia.

There are several possibilities that could mislead this analysis. The first possibility is large estimated uncertainties. However, the dispersion of colour residuals is significantly larger than the estimated uncertainties even if we select medium SNe Ia with smaller uncertainties ($\sigma_{M_B}, \sigma_{M_V} < 0.05$ mag; see Fig. 13). The second possibility is that the two types of SNe Ia correspond to the medium SNe Ia with larger $s_{(B)}$ and smaller $s_{(B)}$, because the $s_{(B)}$ range of the medium SNe Ia is too wide to regard it as a homogeneous sample. However, the tendency is the same for the medium SNe Ia subsamples divided into four groups based on the B-band stretch factor ($0.90 \leq s_{(B)} < 0.95$, $0.95 \leq s_{(B)} < 1.00$, $1.00 \leq s_{(B)} < 1.05$, $1.05 \leq s_{(B)} < 1.10$; see Fig. 14). The result of the Kolmogorov–Smirnov test shows that the distributions of the medium SNe Ia with

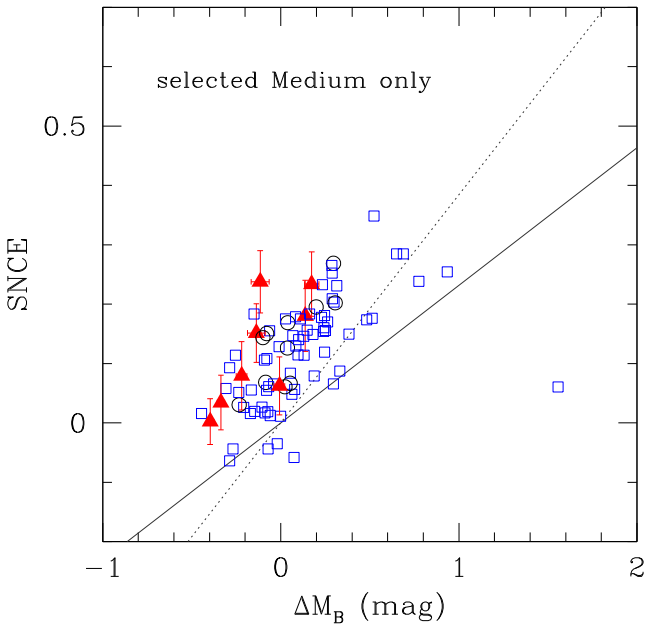

Figure 13. A relation between ΔM_B from the stretch–magnitude relation and SNCE from the stretch–colour relation of the selected medium SDSS SNe Ia with small uncertainties ($0.9 < s_{(B)} \leq 1.1$, $\sigma_{M_B}, \sigma_{M_V} < 0.05$ mag). The symbols and lines are the same as in Fig. 10 (error bars are added to the red host SNe Ia).

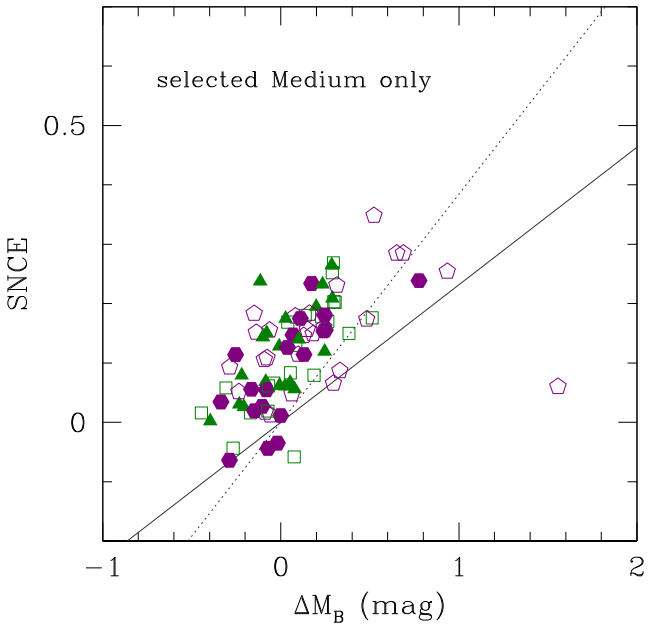

Figure 14. A relation between ΔM_B and SNCE of the selected medium SDSS SNe Ia divided into four groups due to a stretch factor. Green filled triangles are the SNe Ia with $0.90 < s_{(B)} \leq 0.95$, green squares are the SNe Ia with $0.95 < s_{(B)} \leq 1.00$, purple pentagons are the SNe Ia with $1.00 < s_{(B)} \leq 1.05$ and purple filled hexagons are the SNe Ia with $1.05 < s_{(B)} \leq 1.10$. The lines are the same as in Fig. 10.

smaller $s_{(B)}(0.90 \leq s_{(B)} < 0.95)$ and that of the medium SNe Ia with larger $s_{(B)}(1.05 \leq s_{(B)} < 1.10)$ are not different (p-value = 0.28). The third possibility is that the inverse stretch–magnitude relation ($M_B = 1.71 \times s_{(B)}^{-1} - 20.73$), which is used for deriving ΔM_B, creates two apparent subgroups. However, we have confirmed that there is no significant difference (∼1 per cent) between the medium SNe Ia subsamples based on the inverse and normal stretch–magnitude relation.

Table 10. Difference of the properties of host galaxies between the SNLS sample used in Sullivan et al. (2010) and the SDSS sample. The average values of the SNLS sample are calculated from Table 1, except for metallicity, which is read from fig. 9 of Sullivan et al. (2010).

	SNLS	This work
Redshift	0.64	0.16
Stellar mass (log $M_\odot$)	9.8	10.5
Metallicity [12+log(O/H)]	8.5	8.9
sSFR (log $M_\odot$ yr^{-1})	−9.5	−10.0

From these discussions, we conclude there may be two subgroups of medium SNe Ia, which have intrinsically different colours.

Sullivan et al. (2010) examined the colour–magnitude relation of the SNLS SNe sample. Although fig. 9 of Sullivan et al. (2010) shows basically the same properties as those in Fig. 10, we cannot identify two distinct subgroups as in the medium SDSS sample (top-right panel of Fig. 10). However, their results do not conflict with our findings as we cannot identify two subgroups clearly in the SDSS sample, which includes narrow, medium and broad SNe (see Fig. 10). There is another possible explanation: the difference in the redshift ranges of the samples may affect the results. The redshifts of the SNLS SNe sample are higher than those of our sample, and the properties of host galaxies such as stellar mass, metallicity and sSFR are different between the samples (see Table 10). Two distinct subgroups in the medium SDSS sample may be a result of a variety of stellar populations.

Lampeitl et al. (2010) discussed the relation between the properties of SNe Ia and their host galaxies in the SDSS sample, which includes 110 SNe common to this study. They use SALT2 (Guy et al. 2007) and MLCS2k2 (Jha, Riess & Kirshner 2007) for the parametrization of multiband light curves, and they found that the introduction of the third parameter – a host galaxy type – reduces the luminosity dispersion after the corrections. Brandt et al. (2010) also found strong evidence of two progenitor channels related to the age of SN Ia progenitors from the delay time distribution of the SDSS sample. They also use SALT2 (Guy et al. 2007) for the parametrization of multiband light curves, and they have found that tardy components are luminous SNe Ia with high stretch factors and that prompt components are subluminous SNe Ia with low stretch factors. Even though we use a different light-curve analysis method, as described in Section 3, these results are consistent with our conclusion that there are two subgroups of SNe Ia depending on the host galaxy colour.

6.2 Extinction law of host galaxy dust

Dust is another possible factor for creating large dispersions in the colour distributions of SNe Ia that appear in blue host and red host galaxies. The colour–colour relations derived from the SDSS sample indicate that the shapes of the extinction curves are similar to those of the Galactic dust. However, the relations between ΔM_B and SNCE, which is related to the conversion factor R, have different implications.

From Fig. 10, it is not clear whether or not the average R_V of host galaxy dust is close to the standard Galactic value ($R_V = 3.3$). As shown in Section 6.1, the SDSS sample may include two types of SNe Ia, which have intrinsically different colours. In order to reduce

the uncertainty of intrinsic diversity of SNe Ia colour, we derive R_V from the medium, broad and narrow samples. As a result, we find that a value of R_V derived from the medium sample is $3.3^{+0.2}_{-0.1}$, and it is consistent with the standard Galactic value. However, values of R_V derived from the medium red host sample ($2.0^{+0.2}_{-0.1}$) and the narrow blue host sample ($2.3^{+0.3}_{-0.3}$) are significantly smaller than the standard Galactic value. These results are consistent with previous studies – e.g. $R_B \sim 3.5$ (Phillips et al. 1999; Knop et al. 2003; Altavilla et al. 2004), $R_B \sim 3.3$ (Wang et al. 2006), $R_V = 1.75 \pm 0.27$ (Nobili & Goobar 2008) and $R_V = 2.2$ (Kessler et al. 2010) – which find that values of R are smaller than the standard Galactic value.

These measurements may indicate that the value of R_V has a large intrinsic dispersion. Also, we should note that there are large variations of the interstellar extinction curve, even in our Galaxy (Nataf et al. 2016). An example is given by Folatelli et al. (2010), who found $R_V \approx 1.7$ for their sample of SNe Ia, but this value changed to $R_V \approx 3.2$ if the highly reddened SNe were excluded.

6.3 Other factors that may have affected the observed SNe Ia colours

In the line of sight towards any SN Ia, there may be circumstellar dust (CSD) around the SN Ia in addition to dust in the interstellar medium (ISM). The existence of circumstellar material (CSM) is expected based on theoretical arguments (e.g. Nomoto 1982; Hachisu, Kato & Nomoto 1999), and several recent observations have indicated the existence of circumstellar gas around spectroscopically normal SNe Ia: e.g. SN2000cx (Mazzali et al. 2005; Patat et al. 2007a), SN2002ic (Hamuy et al. 2003), SN2003du (Germany et al. 2004), SN2005cg (Quimby et al. 2006), SN2006X (Patat et al. 2007b), SN2007af (Simon et al. 2007), SN2012ca and SN2013dn (Fox et al. 2015). Wang (2005) reported the possibility that CSD associated with circumstellar gas has a smaller value of R_V than that of Galactic ISM. Smaller R values normally indicate a smaller size of dust particles (see Draine 2003). Wang (2005) also pointed out that a low R_V of host galaxy dust estimated from SNe Ia may be a result of the reflection effect from CSD. The distribution, in which the SNe appearing in red host galaxies (red triangles in Fig. 10) are plotted along a low R_V line, can be explained by these ideas.

New observations provide increasing evidence suggesting the presence of CSM/CSD in (at least some of) SNe Ia. Blondin et al. (2009) detected variable Na I D lines in the low-resolution spectra of SN1999cl and SN2006X, suggesting that the variability could be associated with interstellar absorption. Sternberg et al. (2011) showed that the sodium absorption features in the 35 SNe Ia they observed indicate the presence of CSM around the progenitor system, which may have originated from gas outflows from single-degenerate progenitors. Later, Dilday et al. (2012) reported a complex, multishell CSM structure in the close environment of SN Ia PTF 11kx. An RS Oph-like symbiotic nova progenitor was proposed for this particular SN. Further, Förster et al. (2012, 2013) put forward new evidence for the presence and asymmetric distribution of CSM in SNe Ia from the observations of nearby SNe Ia. Also recently, Johansson, Amanullah & Goobar (2013) obtained strict upper limits for the amount of dust around three nearby SNe Ia down to $M_{\rm dust} \lesssim 7 \times 10^{-3}$ $M_\odot$ with *Herschel Space Observatory* far-infrared observations, but they could not completely rule out CSD as one contributor to the reddening suffered by SNe Ia.

Another possible factor affecting the observed SN Ia colour is the viewing angle of the asymmetric SN explosion. An off-centre

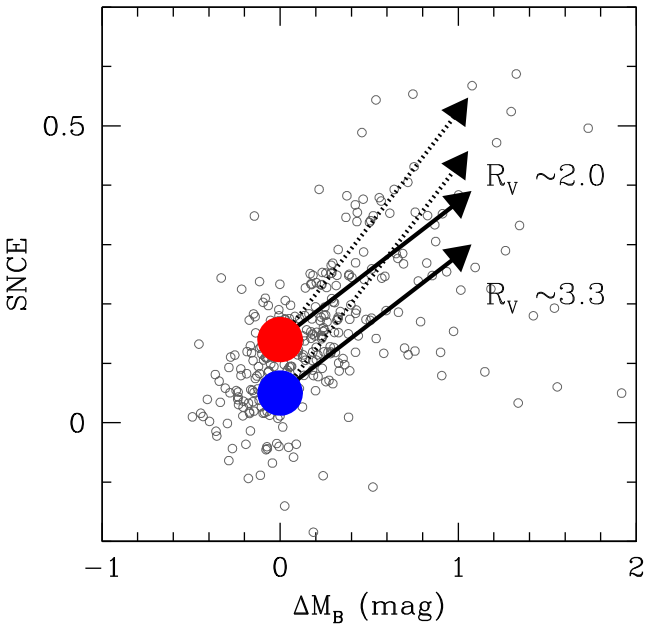

Figure 15. A schematic picture of our conclusion based on the discussion in Section 6. There are two types of SNe Ia with different intrinsic colours (circles), and they are affected by dust with different extinction laws (arrows). The solid line denotes the conversion factor of standard Galactic extinction ($R_V = 3.3$) and the dotted line denotes a smaller conversion factor ($R_V = 2.0$). Grey small circles are the SDSS sample, as in the top-left panel of Fig. 10, which probably includes a mixture of these factors.

explosion of the white dwarf progenitor star in a SN Ia (Maeda et al. 2010) may affect the luminosity and colour of the SN (Maeda et al. 2011; Cartier et al. 2011). SNe viewed from the side closer to the ignition centre will appear bluer, and those viewed from the other side will appear redder. Maeda et al. (2011) shows a difference of the peak luminosity changes ∼30 per cent due to the viewing angle. The colour of the SN also seems to be correlated with the ejecta velocity (Foley & Kasen 2011; Foley 2012), with high-velocity SNe tending to be redder than low-velocity SNe, and the offset is ∼0.04 mag. As we discussed in Section 6.1, if the SNe appearing in red host galaxies, except for dust-rich late-type galaxies, are all tardy SNe Ia, then the viewing angle is one possible explanation for their distribution in Fig. 10. Nevertheless, we cannot conclude that dependence on the ejecta velocity is seen in our sample.

While, with the current photometric data set, we are unable to address the aforementioned points affecting the colours of our SNe, disregarding those possible factors we present the empirical result of our study as follows. A schematic picture of our conclusion based on the discussion above is shown in Fig. 15. There may be two types of SNe Ia with different intrinsic colours, and their colours are affected by dust with two different extinction properties.

This idea does not conflict with Scolnic et al. (2014), who pointed out that the Galactic reddening law ($R_v = 3.1$) can explain the trend between Hubble residuals and colours. As we show in Table 7, the reddening law ($R_v = 3.3$) derived from the medium sample is consistent with the Galactic reddening law. The smaller value of R_v can be derived if we regard the SN sample as two components, as we have discussed.

6.4 Implications for cosmology

If there are two subgroups of medium SNe Ia, which have intrinsically different colours, and they are made extinct by host galaxy dust

with different properties, what are the implications for cosmological studies?

The offset in intrinsic colour between two subgroups of medium SNe Ia is 0.06 mag, as we have shown in Section 6.1. This colour offset becomes $\Delta M_B = 0.26$ mag under the standard galactic extinction law ($R_B = 4.3$). This is a significantly large value compared with the standard value of peak brightness dispersion $\sigma_{M_B} \sim 0.15$. However, because the medium SNe appearing in red host galaxies are only 13 per cent of all the medium SNe (28 out of 208), the large offset is smoothed when we use a SN sample with no selection bias. However, when we use a SNe sample selected by host galaxy type, it should be carefully analysed as the offset may become a factor of systematic uncertainty. If there are statistically enough medium SNe appearing in red host galaxies, then the dispersion of peak brightness is expected to be smaller than that of all medium SNe.

In order to reduce uncertainty due to the variety of R_V, we should use only the bluest SNe Ia for cosmological studies, unless we know a proper R_V of each supernova. However, it is necessary to carefully select the bluest SNe Ia subsample when we use them. If we assume that a SN with $-0.2 \leq M_B - M_V \leq -0.1$ is the bluest SN, then these are 13 per cent of all the medium SNe (28 out of 208). This colour-selected sample reduces systematic uncertainties in luminosity estimation by a factor of 2, but the small number of the sample results in increasing statistical uncertainties. As we show in Table 8, the effects are cancelled in this study (i.e. the dispersion of medium sample B subsamples is similar in spite of the difference in sample size).

When we have a larger SNe Ia sample in future, the use of subsamples of carefully selected SNe Ia may improve the precision of the cosmological measurements with SNe Ia. Cosmological studies are not the main topic in this paper, but the current study may become helpful for optimized sample selection.

7 SUMMARY

In this paper, we present the photometric properties of the intermediate-redshift SNe Ia found by the SDSS-II SN Survey. The *u*-, *g*-, *r*-, *i*- and *z*-band light curves of the SDSS SNe Ia are parametrized into rest-frame *U*-, *B*-, *V*-, *R*- and *I*-band stretch factors, peak luminosities and *B*-band maximum luminosity dates using the multiband stretch method, which can simply parametrize light-curve shapes and peak brightness without any additional assumptions such as dust extinction models, unlike the widely used methods SALT2 and MLCS.

Considering the observational uncertainties and selection biases, we select 328 SNe Ia in the range $0.05 \leq z < 0.24$ for a study of their photometric properties. Applying the stretch–magnitude and stretch–colour relations derived from the SDSS sample, we find that most of the SNe Ia that appeared in red host galaxies do not have a broad light curve, whereas the SNe Ia that appeared in blue host galaxies have a variety of light-curve widths. The Kolmogorov–Smirnov test shows that the SNe Ia of these two subsamples selected by the host galaxy colour have significantly different colours (significance level of 99.9 per cent).

We infer that tardy SNe Ia appeared in both red host and blue host galaxies but prompt SNe Ia appeared in only blue host galaxies. Based on the inference, the medium and narrow SNe Ia appearing in red host galaxies are pure tardy samples, and the broad SNe Ia appearing in blue host galaxies are pure prompt samples. Both of these pure samples have a smaller dispersion ($\leq$0.06 mag) in the SNCE around the best-fitting relation than the medium and narrow SNe Ia appearing in blue host galaxies, which are expected to be a mixture of tardy and prompt SNe Ia.

We also investigate the extinction law of host galaxy dust. As a result, we find that a value of R_V derived from the medium sample is $3.3^{+0.2}_{-0.1}$, and it is consistent with the standard Galactic value. However, values of R_V derived from the medium, red host sample ($2.0^{+0.2}_{-0.1}$) and narrow, blue host sample ($2.3^{+0.3}_{-0.3}$) are significantly smaller than the standard Galactic value.

These results indicate that there may be two types of SNe Ia with different intrinsic colours, and they are made extinct by host galaxy dust with two different properties. This idea does not claim a review of cosmological studies with an unbiased SNe Ia sample. However, there is a possibility that the systematic uncertainty could be reduced by selecting SNe Ia based on this idea.

ACKNOWLEDGEMENTS

Funding for the creation and distribution of the SDSS and SDSS-II has been provided by the Alfred P. Sloan Foundation, the Participating Institutions, the National Science Foundation, the US Department of Energy, the National Aeronautics and Space Administration, the Japanese Monbukagakusho, the Max Planck Society and the Higher Education Funding Council for England. The SDSS web site is http://www.sdss.org/. This work was also supported in part by a Japan Society for the Promotion of Science (JSPS) core-to-core programme, 'International Research Network for Dark Energy', and by a JSPS research grant. We also acknowledge support by CONICYT through FONDECYT grant 3140563, and by Project IC120009 'Millennium Institute of Astrophysics (MAS)' of the Iniciativa Científica Milenio del Ministerio de Economía, Fomento y Turismo de Chile.

The SDSS is managed by the Astrophysical Research Consortium for the Participating Institutions. The Participating Institutions are the American Museum of Natural History, Astrophysical Institute Potsdam, University of Basel, Cambridge University, Case Western Reserve University, University of Chicago, Drexel University, Fermilab, the Institute for Advanced Study, the Japan Participation Group, Johns Hopkins University, the Joint Institute for Nuclear Astrophysics, the Kavli Institute for Particle Astrophysics and Cosmology, the Korean Scientist Group, the Chinese Academy of Sciences (LAMOST), Los Alamos National Laboratory, the Max-Planck-Institute for Astronomy (MPA), the Max-Planck-Institute for Astrophysics (MPiA), New Mexico State University, Ohio State University, University of Pittsburgh, University of Portsmouth, Princeton University, the United States Naval Observatory and the University of Washington.

This work is based in part on observations made at the following telescopes. The Hobby–Eberly Telescope (HET) is a joint project of the University of Texas at Austin, Pennsylvania State University, Stanford University, Ludwig-Maximillians-Universität München and Georg-August-Universität Göttingen. The HET is named in honour of its principal benefactors, William P. Hobby and Robert E. Eberly. The Marcario Low-Resolution Spectrograph is named for Mike Marcario of High Lonesome Optics, who fabricated several optical elements for the instrument but died before its completion; it is a joint project of the HET partnership and the Instituto de Astronomía de la Universidad Nacional Autónoma de México. The Apache Point Observatory 3.5-m telescope is owned and operated by the Astrophysical Research Consortium. We thank the observatory director, Suzanne Hawley, and site manager, Bruce Gillespie, for their support of this project. The Subaru Telescope is operated by the National Astronomical Observatory of Japan. The

William Herschel Telescope is operated by the Isaac Newton Group on the island of La Palma in the Spanish Observatorio del Roque de los Muchachos of the Instituto de Astrofisica de Canarias. The W. M. Keck Observatory is operated as a scientific partnership among the California Institute of Technology, the University of California, and the National Aeronautics and Space Administration. The Observatory was made possible by the generous financial support of the W. M. Keck Foundation.

This research has made use of the NASA/IPAC Extragalactic Database (NED) which is operated by the Jet Propulsion Laboratory, California Institute of Technology, under contract with the National Aeronautics and Space Administration.

We thank the SDSS collaborators for discussions and meaningful suggestions regarding this work. We also thank Michael Richmond for carefully reading the manuscript.

REFERENCES

Altavilla G. et al., 2004, MNRAS, 349, 1344
Astier P. et al., 2006, A&A, 447, 31
Benetti S. et al., 2005, AJ, 623, 1011
Betoule M. et al., 2014, A&A, 568, 22
Blanton M. R., Berlind A. A., 2007 ApJ, 664, 791
Blondin S., Prieto J. L., Patat F., Challis P., Hicken M., Kirshner R. P., Matheson T., Modjaz M., 2009, ApJ, 693, 207
Branch D., Fisher A., Nugent P., 1993, AJ, 106, 2383
Brandt T. D., Tojeiro R., Aubourg É., Heavens A., Jimenez R., Strauss M. A., 2010, AJ, 140, 804
Cardelli J. A., Clayton G. C., Mathis J. S., 1989, ApJ, 345, 245
Cartier R., Förster F., Coppi P., Hamuy M., Maeda K., Pignata G., Folatelli G., 2011, A&A, 534, L15
Dilday B. et al., 2008, ApJ, 682, 262
Dilday B. et al., 2012, Science, 337, 942
Doi M. et al., 2010, AJ, 139, 1628
Draine B. T., 2003, ARA&A, 41, 241
Ellis R. S. et al., 2008, ApJ, 674, 51
Filippenko A. V., 2005, ASSL, 332, 97
Filippenko A. V. et al., 1992, AJ, 104, 1543
Folatelli G. et al., 2010, AJ, 139, 120
Foley R. J., 2012, ApJ, 748, 127
Foley R. J., Kasen D., 2011, ApJ, 729, 55
Foley R. J. et al., 2008a, ApJ, 684, 68
Foley R. J., Filippenko A. V., Jha S. W., 2008b, ApJ, 686, 117
Förster F., González-Gaitán S., Anderson J., Marchi S., Gutiérrez C., Hamuy M., Pignata G., Cartier R., 2012, ApJ, 754, L21
Förster F., González-Gaitán S., Folatelli G., Morrell N., 2013, ApJ, 772, 19
Fox O. D. et al., 2015, MNRAS, 447, 772
Frieman J. A. et al., 2008, AJ, 135, 338
Fukugita M., Ichikawa T., Gunn J. E., Doi M., Shimasaku K., Schneider D. P., 1996, AJ, 111, 1748
Galbany L. et al., 2012, ApJ, 755, 125
Germany L. M., Reiss D. J., Schmidt B. P., Stubbs C. W., Suntzeff N. B., 2004, A&A, 415, 863
Goldhaber G. et al., 2001, ApJ, 558, 359
Gunn J. E. et al., 1998, AJ, 116, 3040
Gunn J. E. et al., 2006, AJ, 131, 2332
Guy J. et al., 2007, A&A, 466, 11
Hachisu I., Kato M., Nomoto K., 1999, ApJ, 522, 487
Hamuy M., Phillips M. M., Wells L. A., Maza J., 1993, PASP, 105, 787
Hamuy M., Phillips M. M., Maza J., Suntzeff N. B., Schommer R. A., Aviles R., 1995, AJ, 109, 1
Hamuy M. et al., 1996a, AJ, 112, 2408 (HAM96)
Hamuy M., Phillips M. M., Suntzeff N. B., Schommer R. A., Maza J., Aviles R., 1996b, AJ, 112, 2391
Hamuy M., Trager S. C., Pinto P. A., Phillips M. M., Schommer R. A., Ivanov V., Suntzeff N. B., 2000, AJ, 120, 1479
Hamuy M. et al., 2003, Nature, 424, 651
Hicken M., Wood-Vasey W. M., Blondin S., Challis P., Jha S., Kelly P. L., Rest A., Kirshner R. P., 2009, ApJ, 700, 1097
Holtzman J. A. et al., 2008, AJ, 136, 2306
Howell D. A., 2001, ApJ, 554, L193
Hsiao E. Y., Conley A., Howell D. A., Sullivan M., Pritchet C. J., Carlberg R. G., Nugent P. E., Phillips M. M., 2007, ApJ, 663, 1187
James J. B., Davis T. M., Schmidt B. P., Kim A. G., 2006, MNRAS, 370, 933
Jha S. et al., 2006, AJ, 131, 527 (JHA06)
Jha S., Riess A. G., Kirshner R. P., 2007, ApJ, 659, 122
Johansson J., Amanullah R., Goobar A., 2013, MNRAS, 431, L43
Jones D. O., Riess A. G., Scolnic D. M., 2015, ApJ, 812, 31J
Kelly P. L., Hicken M., Burke D. L., Mandel K. S., Kirshner R. P., 2010, ApJ, 715, 743
Kessler R. et al., 2010, ApJ, 717, 40
Kim A., Goobar A., Perlmutter S., 1996, PASP, 108, 190
Knop R. A. et al., 2003, ApJ, 598, 102
Lampeitl H. et al., 2010, ApJ, 722, 566
Leibundgut B. et al., 1993, AJ, 105, 301
Maeda K. et al., 2010, Nature, 466, 82
Maeda K. et al., 2011, MNRAS, 413, 3075
Mannucci F., Della V. M., Panagia N., Cappellaro E., Cresci G., Maiolino R., Petrosian A., Turatto M., 2005, A&A, 433, 807
Mannucci F., Della V. M., Panagia N., 2006, MNRAS, 370, 773
Mazzali P. A. et al., 2005, ApJ, 623, L37
Nataf D. M. et al., 2016, MNRAS, 456, 2692
Neill J. D. et al., 2009, ApJ, 707, 1449
Nobili S., Goobar A., 2008, A&A, 487, 19
Nomoto K., 1982, ApJ, 253, 798
Nugent P., Phillips M., Baron E., Branch D., Hauschildt P., 1995, ApJ, 455, L147
Nugent P., Kim A., Perlmutter S., 2002, PASP, 114, 803
Patat F. et al., 2007a, A&A, 474, 931
Patat F. et al., 2007b, Science, 317, 924
Perlmutter S. et al., 1997, in Ruiz-Lapuente P., Canal R., Isern J., eds, Thermonuclear Supernova. Dordrecht, Kluwer, p. 749
Perlmutter S. et al., 1999, ApJ, 517, 565
Phillips M. M., 1993, ApJ, 413, L105
Phillips M. M., Wells L. A., Suntzeff N. B., Hamuy M., Leibundgut B., Kirshner R. P., Foltz C. B., 1992, AJ, 103, 1632
Phillips M. M., Lira P., Suntzeff N. B., Schommer R. A., Hamuy M., Maza J., 1999, AJ, 118, 1766
Quimby R., Höflich P., Kannappan S. J., Rykoff E., Rujopakarn W., Akerlof C. W., Gerardy C. L., Wheeler J. C., 2006, ApJ, 636, 400
Quimby R., Hoflich P., Wheeler J. C., 2007, ApJ, 666, 1083
Riess A. G., Press W. H., Kirshner R. P., 1996, ApJ, 473, 88
Riess A. G. et al., 1998, AJ, 116, 1009
Riess A. G. et al., 1999, AJ, 117, 707 (RIE99)
Rigault M. et al., 2013, A&A, 560, 66
Rigault M. et al., 2015, ApJ, 802, 20
Sako M. et al., 2008, AJ, 135, 348
Sako M. et al., 2011, ApJ, 738, 162
Sako M. et al., 2014, ApJS, preprint (arXiv:1401.3317)
Scannapieco E., Bildsten L., 2005, ApJ, 629, L85
Schlegel D. J., Finkbeiner D. P., Davis M., 1998, ApJ, 500, 525
Schmidt B. P. et al., 1998, ApJ, 507, 46
Scolnic D., Riess A. G., Foley R. J., Rest A., Rodney S. A., Brout D. J., Jones D. A., 2014, ApJ, 780, 37
Simon J. D. et al., 2007, ApJ, 671, L25
Skibba R. A., Bamford S. P., Nichol R. C., Lintott C. J., Andreescu D., Edmondson E. M., Murray P., Raddick M. J., 2009, MNRAS, 399, 966
Smith M. et al., 2012, ApJ, 755, 61
Sternberg A. et al., 2011, Science, 333, 856
Strateva I. et al., 2001, AJ, 122, 1861
Sullivan M. et al., 2006, ApJ, 648, 868
Sullivan M. et al., 2010, MNRAS, 406, 782
Takanashi N., Doi M., Yasuda N., 2008, MNRAS, 648, 868 (TAK08)

van den Bergh S., Li W., Filippenko A. V., 2005, PASP, 117, 773
Wang L., 2005, AJ, 635, L33
Wang X., Wang L., Pain R., Zhou X., Li Z., 2006, ApJ, 645, 488
Wolf R. C. et al., 2016, ApJ, 821, 115
York D. G. et al., 2000, AJ, 120, 1579
Zheng C. et al., 2008, AJ, 135, 1766

SUPPORTING INFORMATION

Supplementary data are available at *MNRAS* online.

Table 5. The sample of the fitting parameters of the 328 intermediate redshift SDSS SNe Ia.

This paper has been typeset from a TEX/LATEX file prepared by the author.